ELSEVIER

Optimal control theory with continuously distributed target states: An application to NaK

Andreas Kaiser, Volkhard May *

Humboldt-Universität zu Berlin, Institut für Physik, Newtonstraße 15, D-12489 Berlin, Germany

Abstract

Laser pulse control of molecular dynamics is studied theoretically by using optimal control theory. The control theory is extended to target states which are distributed in time as well as in a space of parameters which are responsible for a change of individual molecular properties. This generalized treatment of a control task is first applied to wave packet formation in randomly oriented diatomic systems. Concentrating on an ensemble of NaK molecules which are not aligned the control yield decreases drastically when compared with an aligned ensemble. Second, we demonstrate for NaK the maximization of the probe pulse transient absorption in a pump–probe scheme with an optimized pump pulse. These computations suggest an overall optical control scheme, whereby a flexible technique is suggested to form particular wave packets in the excited state potential energy surface. In particular, it is shown that considerable wave packet localization at the turning points of the first-excited Σ-state potential energy surfaces of NaK may be achieved. The dependency of the control yield on the probe pulse parameters is also discussed.
© 2005 Elsevier B.V. All rights reserved.

1. Introduction

Although there are recent experimental demonstrations on possible laser pulse control of polyatomic systems [1–5] the interest in simple systems continues, too. At least, diatomic molecules should offer the best chance to achieve a direct comparison between experimental data and theoretical simulations (see, e.g. [6]). First of all, the success of such a comparison depends on the quality the molecular dynamics have been described. However, in carrying out such a comparison a number of difficulties have to be accounted for caused by the concrete experimental arrangement. These difficulties are mainly related to the fact that, so far, laser pulse control cannot be carried out as a *single molecule* experiment. Instead, the pulse which should drive the molecular dynamics in the required manner acts on a large ensemble of molecules. Accordingly, the spatial intensity profile of the pulse as well as its intensity fluctuations (among different laser shots) may influence the control yield. A similar effect has to be expected when considering molecular ensembles with random spatial orientation or characterized by inhomogeneous broadening. Moreover, what can really be achieved in the experiment may also depend on details of the pulse shaping equipment and the way one tries to detect whether or not the excited molecule has reached the target state.

The effect of the intensity profile of the pulse has been addressed in [7] and the influence of intensity fluctuations, for example, in [8]. Inhomogeneous broadening could be included in the studies of [9], and the influence of the pixel number of the liquid crystal spatial light modulator on the control yield was quantified in [10]. Own recent studies discussed the direct optical detection of the control yield (within a pump probe scheme)

---

* Corresponding author.
  E-mail address: may@physik.hu-berlin.de (V. May).

[11,12]. These considerations will be exemplified here for NaK molecules, and, additionally, it is demonstrated how random spatial orientation of the molecules alters the control yield.

Of course, the different ways the control task is solved in the experiment as well as within numerical simulations may affect the comparability, too. While in the experiment non-deterministic approaches like genetic algorithms are used, optimal control theory (OCT, cf. e.g. [13–16]) is routinely applied within the simulations. It results in a nonlinear functional equation for the laser field (the optimal pulse) which should be ready to solve the control task. We do not further comment on this problem here but will use OCT consequently. The paper is organized as follows. In the subsequent section we give some general comments on OCT, and we shortly introduce the model used for NaK. Then, in Section 3, laser pulse control is investigated in detail if an ensemble of molecules with random spatial orientation is considered. The distribution of the target state in time is considered in Section 4, a situation, one meets in a pump–probe scheme if one directly tries to optimize the probe pulse transient absorption signal. The paper ends with some concluding remarks.

2. Optimal control theory

To achieve laser pulse control one has to optimize a certain molecular property or observable denoted by $\mathcal{O}[E_c]$ in the following. Usually, the applied field (the control field) E_c acts in the time interval (t_0, t_f), and the value of $\mathcal{O}[E_c]$ obtained after optimization is named *control yield*. Because $\mathcal{O}[E_c]$ results from the laser pulse driven dynamics, it is a functional of E_c. Here, and in the following we will provide linear polarization of the control field, so the vectorial field is denoted as

$$\mathbf{E}_c = \mathbf{e}E_c(t), \tag{1}$$

where $\mathbf{e}$ is the polarization unit vector. When applying OCT one searches for an E_c which leads to an extremum of the overall control functional

$$J[E_c] = \mathcal{O}[E_c] - \lambda \left(\frac{1}{2} \int_{t_0}^{t_f} dt \frac{E_c^2(t)}{s(t)} - I_0 \right). \tag{2}$$

The second term represents the constraint to ensure finite control field flux fixed by the value I_0. Moreover, the quantity λ is as Lagrange multiplier, and $s(t)$ guarantees that E_c is switched on and off smoothly. The field pulse E_c resulting in an extremum of $\mathcal{O}[E_c]$ will be called the *optimal* field.

If one restricts the considerations to pure state dynamics, OCT has to be put into the framework of a wavefunction formulation with $\mathcal{O}$ taken as

$$\mathcal{O}[E_c] = \langle \Psi(t; E_c) | \widehat{O} | \Psi(t; E_c) \rangle. \tag{3}$$

Here, $\widehat{O}$ represents an observable which expectation value has to be optimized, and $\Psi(t; E_c)$ is the system wavefunction propagated at the presence of the control field. In the most simple case $\widehat{O}$ is given by the projector $|\Psi_{tar}\rangle\langle\Psi_{tar}|$ on that state to be realized at $t = t_f$ (the target state).

In the following the more general type of the functional $\mathcal{O}$ will be discussed, denoted by

$$\mathcal{O}[E_c] = \int_{t_0}^{\infty} dt \int dp \langle \Psi(t; p) | \widehat{O}(t; p) | \Psi(t; p) \rangle, \tag{4}$$

where p is a certain parameter or set of parameters, which should refer to a particular property changing among the individual molecules. Therefore, the control functional, Eq. (4) accounts for a distribution of the operator $\widehat{O}$ (target state) in the space of the parameter p, and, additionally, in time. Obviously, $\widehat{O}(t; p) = \delta(t - t_f)\delta(p - p_0) \ \widehat{O}$ results in the standard form of $\mathcal{O}[E_c]$ given in Eq. (3). If one takes, however, $\widehat{O}(t; p) = \delta(t - t_f)\widehat{O}(p)$ the functional $\mathcal{O}[E_c]$ is ready to describe, for example, inhomogeneous broadening present in the considered molecular system. In this case p counts the individual molecules which property, for example, the excitation spectrum, changes from molecule to molecule. Consequently, it is required to discuss a distribution of wavefunction in the p-parameter space [9] (cf. also the discussion in Section 3). If, additionally, the target operator is distributed in time the control functional may be used for the optimization of the probe-pulse signal in a pump–probe scheme [11] (see Section 4).

The determination of the optimal control field is achieved by searching for the extremum of J via the solution of $\delta J/\delta E_c = 0$. Using the standard expression Eq. (3) for $\mathcal{O}[E_c]$ the functional derivative of the overall control functional, Eq. (2) leads to

$$E_c(t) = -\frac{2s(t)}{\hbar\lambda} \text{Im} \langle \Theta(t; E_c) | \hat{\mu} | \Psi(t; E_c) \rangle. \tag{5}$$

Here, $\hat{\mu} = \mathbf{e}\hat{\boldsymbol{\mu}}$ is the molecular dipole operator projected onto the control-field polarization. Besides the system state vector $|\Psi(t; E_c)\rangle$ propagated forward in time by means of the time-evolution operator $U(t, t_0; E_c)$ (at the presence of E_c) and starting with $|\Psi_0\rangle$ at $t = t_0$, an auxiliary state vector $|\Theta(t; E_c)\rangle$ appears additionally. It has to be propagated backward in time according to the action of $U(t, t_f; E_c)$ starting at $t_f (\geqslant t)$ and with the "initial" state $\widehat{O}|\Psi(t_f; E_c)\rangle$. A solution of Eq. (5) can be achieved by different iterative schemes of forward and backward propagation. We use the one of [17,18] which results in coupled nonlinear Schrödinger equations for forward and backward propagation.

By fixing λ within the iteration scheme a certain value for the flux $\int dt E_c^2$ is obtained which would be different from I_0, Eq. (2). However, to get a solution for a given I_0 one has to assume J as a function of λ, too. Noting

Eq. (5) a relation between λ and I_0 valid for a given $|\Psi(t)\rangle$ and $|\Theta(t)\rangle$ can be established. It reads

$$\lambda^2 = \hbar^2 I_0/4 \int \mathrm{d}t\, s(t)(\mathrm{Im}\langle\Theta(t)|\hat{\mu}|\Psi(t)\rangle)^2, \qquad (6)$$

and guarantees that the field flux constrain is satisfied. Accordingly, we modify the iteration algorithm such that after each backward and forward propagation step the actual state vectors $|\Psi^{(n)}(t)\rangle$ and $|\Theta^{(n)}(t)\rangle$ of the n'th iteration order are used to estimate the Lagrange multiplier $\lambda^{(n+1)}$ for the next propagation step. For this estimation Eq. (6) is applied, and the iteration procedure is terminated as soon as the control yield (given by $\mathcal{O}$) and the $\lambda^{(n)}$ converge (cf. also [19]).

Now, let us consider OCT based on the more general functional, Eq. (4). In this case the optimal pulse has to be determined from

$$E_{\mathrm{c}}(t) = -\frac{2s(t)}{\hbar\lambda} \int \mathrm{d}p\, \mathrm{Im}\langle\widetilde{\Theta}(t;p,E_{\mathrm{c}})|\hat{\mu}|\Psi(t;p,E_{\mathrm{c}})\rangle. \qquad (7)$$

The integral with respect to the parameter p points out that OCT has to search for a pulse which represents a compromise among the different target operators distributed in the p-parameter space. The distribution of the target operators in time is accounted for by the auxiliary state vector $|\widetilde{\Theta}(t;p,E_{\mathrm{c}})\rangle$ depending on p, too. Again it follows from a backward propagation. However, the definition is more complex as that of $|\Theta\rangle$ appearing in Eq. (5)

$$|\widetilde{\Theta}(t;p,E_{\mathrm{c}})\rangle$$
$$= \int_{t_0}^{\tau_{\mathrm{f}}} \mathrm{d}\tau\, \Theta(\tau-t)U(t,\tau;p,E_{\mathrm{c}})\widehat{O}(\tau,p)|\Psi(\tau;p,E_{\mathrm{c}})\rangle. \qquad (8)$$

Obviously, this is not a single backward propagation but a whole sequence starting at different times τ with the τ-integration realizing a distribution of "initial" conditions. This distribution is restricted to $\tau \geqslant t$, and τ_{f} defines an upper time-limit where $\widehat{O}(\tau,p)$ already equals zero. Note, that Eq. (8) is equivalent to

$$\frac{\partial}{\partial t}|\widetilde{\Theta}(t;p,E_{\mathrm{c}})\rangle = -\frac{\mathrm{i}}{\hbar}H(t)|\widetilde{\Theta}(t;p,E_{\mathrm{c}})\rangle - \widehat{O}(t,p)|\Psi(t;p,E_{\mathrm{c}})\rangle, \qquad (9)$$

what represents an effective *inhomogeneous* time-dependent Schrödinger equation (cf. [11,20–24]). It realizes the backward propagation from a time $t = \tau_{\mathrm{f}}$ with vanishing "initial" condition $|\widetilde{\Theta}(\tau_{\mathrm{f}};p,E_{\mathrm{c}})\rangle = 0$. Because of the inhomogeneous term in Eq. (9) this, however, does not result in zero values of the state vector at all times.

The considerations presented so far will be exemplified by an application to NaK molecules in the gas phase as a prototypical diatomic systems investigated in many respects (see, for example, [6,25] and references therein). We consider the $1^1\Sigma^+$, $2^1\Sigma^+$, and $3^1\Sigma^+$ electronic states

of NaK named in the following ground state, first excited state, as well as higher excited stated and abbreviated by $a = g,e,f$, respectively (cf. also Fig. 1). As shown in [25] the related potential energy surfaces (PES) can be very accurately approximated by Morse potentials. The coupling of the molecular system to the laser field is described within the dipole as well as Condon-approximation. Then, the complete Hamiltonian (expanded with respect to the electronic states φ_a) takes the following form:

$$H(t) = \sum_{a,b=g,e,f} (\delta_{a,b}H_a(r) - E(t)d_{ab})|\varphi_a\rangle\langle\varphi_b|. \qquad (10)$$

Here, $E(t)$ is the total electric field-strength polarized along $\mathbf{e}$ (cf. Eq. (1)). When considering a pump–probe scheme $E(t)$ splits into the control pulse (pump pulse) $E_{\mathrm{c}}(t) \equiv E_{\mathrm{pu}}(t)$ and into the probe pulse $E_{\mathrm{pr}}(t)$. The dipole matrix elements are given by $d_{ab} = \langle\varphi_a|\mathbf{e}\hat{\boldsymbol{\mu}}|\varphi_b\rangle$, where $\hat{\boldsymbol{\mu}}$ as well as the field polarization unit vector $\mathbf{e}$ point along the molecular axis. According to [25] we take the following values: $d_{gg} = 2.8$ D, $d_{ee} = 0.25$ D, and $d_{ff} = 1.5$ D, as well as $d_{eg} = 10.0$ D, $d_{fg} = 3.0$ D, and $d_{fe} = 3.75$ D. Furthermore, the zero-temperature case is considered. Thus, the system is set into the ground state $|\Psi(t_0)\rangle = |\chi_{g0}\rangle|\varphi_g\rangle$ initially, with χ_{g0} denoting the vibrational ground-state wave function in the electronic ground-state. In order to determine the time evolution of the laser pulse driven total wavefunction, an expansion with respect to the electron-vibrational states $\varphi_a\chi_{aM}$ is carried out. The expansion coefficients $C_{aM}(t)$ can be taken to compute the electronic level population $P_a(t) = \sum_M |C_{aM}(t)|^2$, or to determine the probability distribution of the vibra-
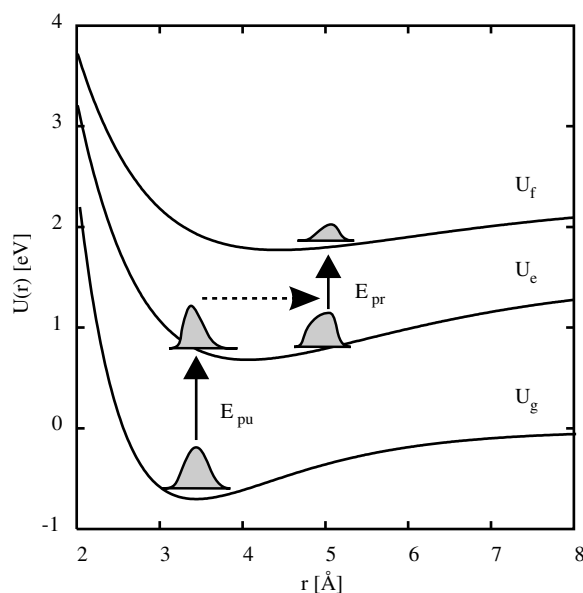

Fig. 1. PES U_g, U_e and U_f of the $1^1\Sigma^+$, $2^1\Sigma^+$, and $3^1\Sigma^+$ electronic states of NaK, respectively (according to [25] the excellent approximation of the PES's by Morse potentials has been taken).

tional coordinate $P_a(r,t) = |\sum_M C_{aM}(t)\chi_{aM}(r)|^2$. Here, this quantity is related to the particular state φ_a and visualizes the respective wave-packet motion.

3. Random orientation of the individual molecules

When considering laser-pulse control in a gas-phase environment the random orientation of the molecules has to be accounted for. Noting the rather large values of the different dipole operator matrix elements of NaK listed in the preceding section one expects that optical transitions are accompanied by rotational excitations. To clearly underline the effect of random orientation on the application of OCT, however, considerations of rotational excitations will be postponed to future studies assuming here a frozen spatial orientation of all molecules considered [26]. As already indicated a given random orientation of the studied molecules can be described by the control functional, Eq. (4) with the parameter p, now, given by the different angles ϑ ($0 \leqslant \vartheta \leqslant \pi$) between the polarization unit vector **e** and the molecular axis. The latter fixes the direction of the dipole moments related to the Σ-states of NaK. Accordingly, the coupling of an individual molecule with a given orientation to the radiation field polarization reads $-E_c(t)\hat{\mu}\cos(\vartheta)$. Since molecules with different spatial orientation "feel" a different overall field-strength the optimal pulse will represent a compromise for the different ways the individual molecule tries to reach the target state.

To achieve a clear indication how this orientational effect influences the control task we consider a target operator $\hat{O}(t;\vartheta)$ which is local in time and which projects on a single target state, i.e. we set $\hat{O}(t;\vartheta) = \delta(t - t_f)|\Psi_{tar}\rangle\langle\Psi_{tar}|$. The target state $|\Psi_{tar}\rangle$ is positioned in the $2^1\Sigma^+$ electronic state (φ_e) such that the molecule is stretched to an Na–K distance of $r = 5.1$ Å at the final time $t_f = 1600$ fs. Therefore, we set $|\Psi_{tar}\rangle = |\chi_e^{(tar)}\rangle|\varphi_e\rangle$, where the vibrational target state $\chi_e^{(tar)}(r)$ is given by the vibrational ground-state wave function $\chi_{e0}(r)$ of the excited state but displaced by $\Delta r = 0.92$ Å. According to the necessary solid angle averaging the quantity $\mathcal{O}$, Eq. (4) now reads

$$\mathcal{O}[E_c] = \frac{1}{2}\int_0^\pi d\vartheta\ \sin(\vartheta)|\langle\chi_e^{(tar)}|\chi_e(t_f;\cos(\vartheta)E_c)\rangle|^2, \quad (11)$$

with the excited-state vibrational wave function $|\chi_e(t_f;\cos(\vartheta)E_c)\rangle = \langle\varphi_e|\Psi(t_f)\rangle$ (note the explicit indication of the ϑ-dependence).

Before discussing the described control task in more detail we note the existence of two excitation intensity regimes, one of weak and one of strong excitation. In the former regime we expect the excited state vibrational wavefunction $\chi_e(t)$ to be proportional to the overall field-strength and thus to $\cos(\vartheta)$. For this weak excita-

tion regime let us assume that the control task has been solved for $\vartheta = 0$. Then, also for those molecules with $\vartheta > 0$, the obtained optimal pulse should move the excited-state vibrational wavefunction into the target state $\chi_e^{(tar)}$, of course with a control yield reduced by $\cos^2(\vartheta)$. Consequently, the overall molecular ensemble control yield is obtained as $\mathcal{O}^{(ref)}[E_c]/3$ with $\mathcal{O}^{(ref)}$ being the reference yield at $\vartheta = 0$. We will demonstrate this behavior in the following and confront it with the case of strong excitation where the behaviour of the differently oriented molecules differs substantially.

In order to solve the variant of Eq. (7) following from $\mathcal{O}$ as specified in Eq. (11) the continuous dependence on ϑ has to be truncated by a discrete set. We consider N different equidistant values ϑ_n ($n = 1, 2, \ldots, N$) of ϑ which are positioned at $\vartheta_n = (n - 1/2)\Delta\vartheta$ (the distance between neighboring values is given by $\Delta\vartheta = \pi/N$). It follows $\mathcal{O}[E_c] = \sum_n w_n|\langle\chi_e^{(tar)}|\chi_e(t_f;\cos(\vartheta_n)E_c)\rangle|^2$, with the pre-factor $w_n = [\cos(\vartheta_n - \Delta\vartheta/2) - \cos(\vartheta_n + \Delta\vartheta/2)]/2$ originated by a partial ϑ-integration (for $N = 1$ we set $w_0 = 1$). Accordingly, it becomes necessary to consider N state vectors for forward propagation and N auxiliary state vectors for backward propagation, all coupled by the discretized version of Eq. (7).

Fig. 2 displays the influence of the extent of discretization on the solution of the control task (note that the used control pulse intensity moves the control task already a little bit out of the weak-excitation regime). Increasing N the control yield strongly decreases, but remains nearly unchanged at $N \approx 4$ and converges for $N \approx 12$. This behavior has to be expected since the optimal control field $E_c(t)$ represents a compromise among those fields which would maximize the control yield for a given orientation. Similar, the shape of the optimal pulse changes with N and converges like the control yield (see the upper panel of Fig. 3). When performing the optimization for one fixed orientation, the optimal pulse slightly differs from that shown in Fig. 3 underlining again that the chosen control pulse intensity of 1 mJ/cm^2 already leads to a deviation from weak-field excitation. It would be of also interest to monitor how the individual molecules behave under the influence of the
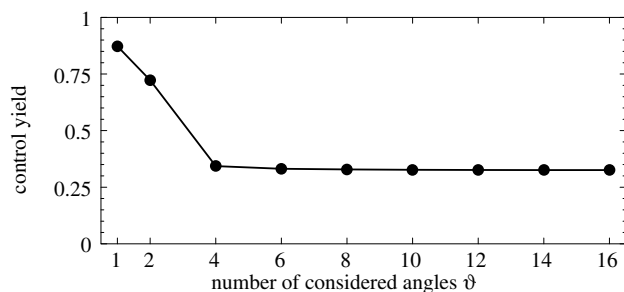

Fig. 2. Control yield as a function of the number of the equidistantly discretized angle ϑ (the computations correspond to control pulse intensity of 1 mJ/cm^2).
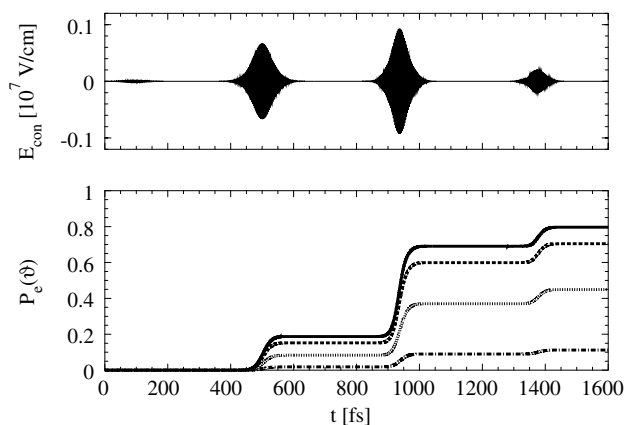
Fig. 3. Optimal field pulse for an ensemble of randomly oriented molecules (upper panel, control task like in Fig. 2 but with fixed penalty factor $\lambda = 1$ and $N = 16$). Populations $P_e(\vartheta)$ of molecules with different orientations ϑ_n as a function of time are shown in the lower panel. Solid line: $\vartheta_1 = 5.6°$, dashed line: $\vartheta_3 = 28.1°$, dotted line: $\vartheta_5 = 50.6°$, and dashed-dotted line $\vartheta_7 = 73.1°$.

optimal pulse which solves the control task for the whole random oriented ensemble. This is shown in Fig. 3 where the time evolution in the excited state φ_e is drawn for different ϑ_n. When ϑ_n moves to $\pi/2$ the coupling to the laser field becomes smaller leading to a smaller overall population transfer into the excited state. But, the wave packet dynamics in all molecules remain similar, i.e. the different $\chi_e(t; \cos(\vartheta_n)E_c)$ when normalized to 1 are nearly identical.

For larger intensities we expect that the temporal behavior of the individual wave packet motion depends on the field strength. This is demonstrated in Fig. 4. In
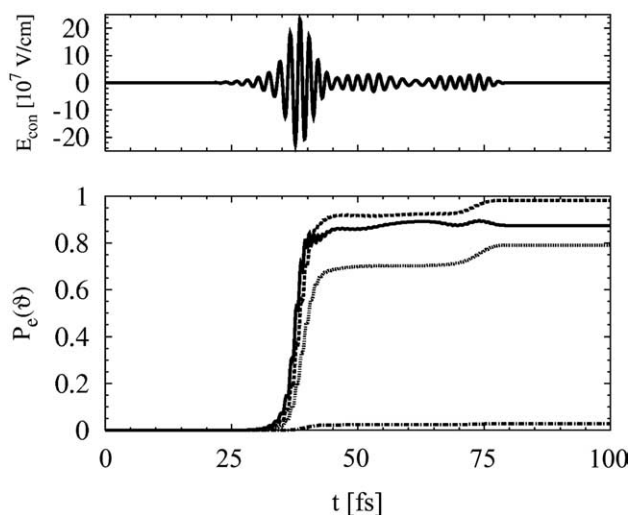

Fig. 4. Optimal field pulse for an ensemble of randomly oriented molecules (upper panel, case of intensive and fast excitation, penalty factor fixed at $\lambda = 0.001$, $N = 20$). The populations $P_e(\vartheta)$ of different oriented molecules as a function of time are shown in the lower panel: $\vartheta_1 = 4.5°$ (solid line), $\vartheta_5 = 40.5°$ (dashed line), $\vartheta_8 = 67.5°$ (dotted line), and $\vartheta_{11} = 94.5°$ (dashed-dotted line).

order to deal with a larger control pulse intensity calculations have been carried out using the three electronic level model of [11] with parabolic PES and larger vibrational frequencies. According to Fig. 4 the population of the excited state becomes largest for molecules with $\vartheta \approx 40°$. Nevertheless, the wave packet dynamics for all orientations do not differ so much. This all indicates that the orientational effect is of less importance when exclusively focusing within OCT on the study of the (vibrational) wave packet dynamics (except for the case of very high control pulse intensities). The consideration of a wavefunction $\chi_e(t)$ obtained by solving the control task for a completely aligned ensemble would give sufficient insight. However, the correct computation of the control yield of a random oriented ensemble cannot be obtained in this way but requires to solve the control task as described.

4. Optimizing the probe-pulse transient absorption signal

Various control experiments focus on an optical signal as an observable to be maximized (cf., e.g. [1–4]). It would be also of interest to consider such a case in the framework of the OCT just discussing an overall optical control scheme. To this end let us consider the maximization of the probe pulse transient absorption signal (TAS) in a pump–probe experiment. It becomes immediately obvious that this problem represents an example for a control task where the target operator (target state) is distributed in time (cf. Eq. (4)). Thereby, we have in mind a pump pulse induced transition into the first excited state which is then probed by a transition into the higher excited state (cf. Fig. 1). Just the fact that the probe pulse has a finite duration indicates that an optimization of a quantity becomes necessary which is determined by the molecular dynamics in a certain time-interval. To specify the control task $\mathcal{O}[E_c]$, Eq. (4) is identified by the TAS

$$S_{pr} = -\int dt \frac{\partial E_{pr}(t)}{\partial t} P_{pr}(t). \tag{12}$$

This expression specifies the TAS as the energy gain (per sample volume) the molecular system experiences at the presence of the probe field. Eq. (12) assumes the vectorial probe field-strength in a slight difference to Eq. (1) as $\mathbf{E}_{pr} = \mathbf{e}_{pr}E_{pr}(t)/\sqrt{2} \times \exp(i\mathbf{k}_{pr}\mathbf{r}) + $ c.c., with polarization unit vector $\mathbf{e}_{pr}$, wave vector $\mathbf{k}_{pr}$ and *real* envelope $E_{pr}(t)$. The polarization field induced by the probe pulse is taken in a similar form with P_{pr} also denoting the real envelope.

To get S_{pr}, Eq. (12) P_{pr} has to be extracted from the total polarization $\mathbf{P} = n_{mol}\langle \Psi(t)|\hat{\boldsymbol{\mu}}|\Psi(t)\rangle$ (n_{mol} is the volume density of the considered molecules and $\Psi(t)$ the laser-driven wavefunction). We follow the treatment of [11] and take the difference between the polarization

calculated at the presence of the pump and probe field as well as at the presence of the pump field only

$$P_{pr}(t) = \frac{n_{mol}\cos(\mathbf{k}_{pr}\mathbf{r})}{\sqrt{2}}\left[\langle\Psi(t;E_{con},E_{pr})|\mathbf{e}_{pr}\hat{\boldsymbol{\mu}}|\Psi(t;E_{con},E_{pr})\rangle\right.$$
$$\left. -\langle\Psi(t;E_{con})|\mathbf{e}_{pr}\hat{\boldsymbol{\mu}}|\Psi(t;E_{con})\rangle\right]. \quad (13)$$

This equation together with Eq. (12) can be used to specify the target operator $\hat{O}(t;p)$ introduced in Eq. (4). It reads

$$\hat{O}(t;p) = -\left(\delta(p-p_{pum+pr}) - \delta(p-p_{pum})\right)\frac{n_{mol}\cos(\mathbf{k}_{pr}\mathbf{r})}{\sqrt{2}}$$
$$\times \frac{\partial E_{pr}(t)}{\partial t}\mathbf{e}_{pr}\hat{\boldsymbol{\mu}}. \quad (14)$$

Besides the continuous time dependence only two values of the p-parameter are necessary, namely p_{pum+pr}, and p_{pum}, indicating in the first case the need to propagate the wave function at the presence of the pump and the probe pulse and in the latter case at the presence of the pump pulse only.

To apply this optimization scheme to NaK a Gaussian-shaped probe pulse with an amplitude of $E_{pr}^{(0)} = 10^{-4}$ V/cm, centered at $t_{pr} = 1600$ fs is used. Its length τ_{pr} (FWHM) is varied between 10 fs and 60 fs. The central frequencies have been chosen as $\hbar\omega_{pr} = 0.83$, 0.85, 0.87, and 0.90 eV. Considering non-overlapping pump and probe pulses, the pump pulse is restricted to the interval between $t_0 = 0$ fs and $t_f = 1500$ fs (with an intensity of 1 mJ/cm^2). For $s(t)$ (cf. Eq. (2)) a sine-square function is applied.

The optimized pump pulse as well as the evolution of the population in the states φ_g and φ_e are shown in Fig. 5 for the optimization of S_{pr} ($\tau_{pr} = 30$ fs and $\hbar\omega_{pr} = 0.85$ eV). As it becomes obvious the pump pulse consists of several sub-pulses, each of them moves population from φ_g into φ_e (the population φ_f is negligible small and has not been plotted). With the first sub-pulse a vibrational wave packet is created in the state φ_e, which propagates across the PES (to be seen as tilted gray lines). Whenever it returns to its original position, its overall magnitude is further increased by one of the next sub-pulses. Correspondingly sub-pulses are 200 fs apart, according to the vibrational period of NaK in the $2^1\Sigma^+$ state (denoted here by φ_e). By this mechanism a localized vibrational wave packet is formed at the right border of the PES when the probe-pulse acts, and the shape of the wave packet is optimized for a transition to the higher-excited state φ_f.

If the probe pulse central frequency is slightly shifted to $\hbar\omega_{pr} = 0.90$ eV significant changes result as shown in Fig. 6. The optimized pump pulse consist of a larger number of sub-pulses compared to that of Fig. 5, and these sub-pulses are grouped in pairs which are 200 fs apart. Accordingly, two subsequent vibrational wave packets are created in the first excited electronic state,
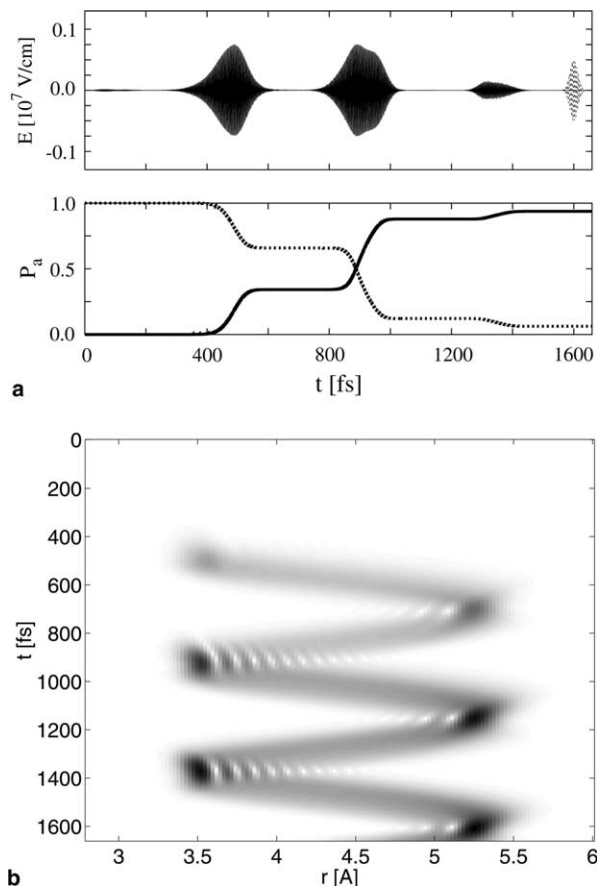

Fig. 5. Optimized TAS, Eq. (12). Upper panel: time dependence of the electric field-strength of the optimal pump pulse (solid line, control pulse intensity equals 1 mJ/cm^2) and of the probe pulse (dotted line, enlarged by a factor of 50, probe pulse parameters: $\hbar\omega_{pr} = 0.85$ eV, and $\tau_{pr} = 30$ fs). Middle panel: electronic ground-state population P_g (dotted line) and excited-state population P_e (solid line) versus time. Lower panel: contour plot of the probability density $P_e(r,t)$ referring to vibrational wave packet motion in the excited state φ_e.

shown as parallel tilted gray lines in Fig. 6. These wave packets interfere such that a localized wave packet is formed within the PES at $r \approx 5$ Å (and during the probe pulse action). The shape and position of this wave packet is suitable for transferring population from φ_e into φ_f using the central frequency of $\hbar\omega_{pr} = 0.90$ eV.

According to the behavior reported so far it is of interest to study the dependence of the optimized TAS on the probe-pulse length τ_{pr} and the carrier frequency ω_{pr}. The results are plotted in Fig. 7 with the TAS rescaled by the probe pulse flux $\int E_{pr}^2(t)\,dt$. For a short probe pulse length ($\leqslant 20$ fs) the rescaled TAS increases linearly with τ_{pr}, and for $\tau_{pr} = 10$ fs, it takes the same value for 0.85 eV $\leqslant \hbar\omega_{pr} \leqslant 0.9$ eV what is caused by the large frequency broadening of such a short pulse. For $\tau_{pr} > 20$ fs the TAS increases slightly sub-linear with τ_{pr}, since the vibrational dynamics prevents the localization of the wave packet during the whole probe pulse. However, there is an optimal ω_{pr} with $\hbar\omega_{pr} \approx 0.87$ eV, where the TAS behaves as in the case of an infinite short
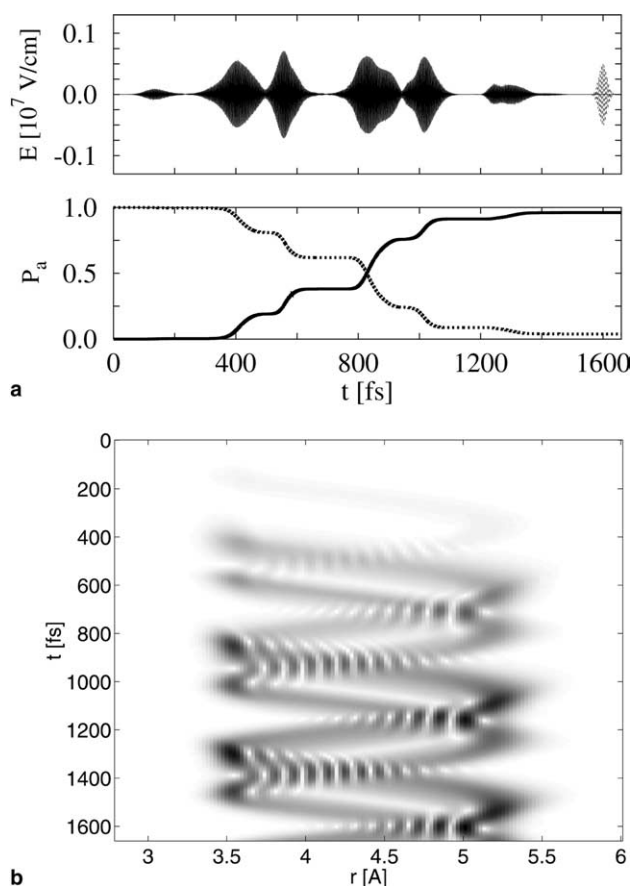
Fig. 6. Optimized TAS, Eq. (12). Upper panel: time dependence of the electric field strength of the optimal pump pulse (solid line, control pulse intensity equals 1 mJ/cm^2) and of the probe pulse (dotted line, enlarged by a factor of 50, probe pulse parameters: $\hbar\omega_{pr} = 0.9$ eV, and $\tau_{pr} = 30$ fs). Middle panel: electronic ground-state population P_g (dotted line) and excited-state population P_e (solid line) versus time. Lower panel: contour plot of the probability density $P_e(r,t)$ referring to vibrational wave packet motion in the excited state φ_e.
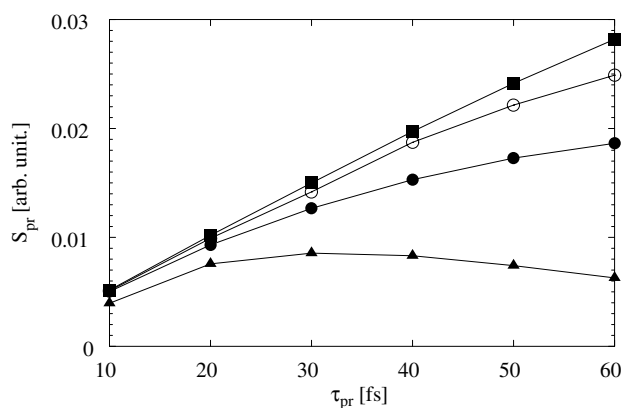

Fig. 7. Rescaled TAS as a function of the probe pulse duration τ_{pr} and the central frequency ω_{pr}. Triangles: $\hbar\omega_{pr} = 0.83$ eV, full circles: $\hbar\omega_{pr} = 0.85$ eV, squares: $\hbar\omega_{pr} = 0.87$ eV, and open circles: $\hbar\omega_{pr} = 0.90$ eV.

probe pulse. Accordingly, the rescaled TAS increases linearly with the probe pulse length up to $\tau_{pr} \approx 50$ fs. For $\hbar\omega_{pr} \approx 0.83$ eV the probe pulse absorption is less resonant and the TAS becomes smaller for all τ_{pr} compared to what has been observed beforehand. Furthermore, the vibrational dynamics becomes more dominant leading to a decrease of the absorption signal already for $\tau_{pr} > 30$ fs.

In order to combine the optimization of the probe-pulse TAS presented here with the considerations of the preceding section by including random orientations of the excited molecules it remains insufficient to follow the scheme of Section 3. Instead, orientational averaging has also to be accounted for when calculating the probe pulse polarization, Eq. (13). The concentration on a weak-excitation regime, as discussed in Section 3, however, should not drastically alter the results obtained here.

5. Summary and conclusions

In order to make a step forward in relating theoretical simulations on laser pulse control of molecular dynamics to respective experiments the OCT has been generalized to the use of target states which are distributed in a particular space of parameters. In this way, first, it became possible to account for effects of static disorder. As a particular example a random oriented ensemble of laser driven molecules has been analyzed in some detail. Considering a target state distribution in time, one may optimize an observable measured in the experiment mandatory within a certain time-interval. As an application the optimization of the TAS of a probe pulse in a pump–probe scheme has been discussed. To achieve clear indications for the effect of target state distributions when calculating the control yield all consideration have been concentrated on simple NaK molecules in a gas-phase situation.

When studying the effect of random spatial orientation of molecules we obtained a considerable decrease of the control yield compared to the case of spatially aligned molecules. This behavior has to be expected because the individual molecules become excited by a control field which decreases with the cosine of the angle between the molecular axis (defining the direction of the transition dipole moment) and the control field polarization. Moreover, when solving the control task, on the one-hand side, for a random orientation and on the other-hand side for a spatial alignment, both optimal pulses differ strongly. But if the overall field-strength for the case of random oriented molecules is not too large the vibrational wave packet dynamics in all molecules are similar. Focusing on it, an orientation averaging becomes not necessary. The averaging is unavoidable, however, when the ensemble control yield is needed for a comparison with experimental data.

Moreover, we discussed the optimization of the probe pulse TAS for NaK molecules after photo excitation by

concentrating on a transition from the $2^1\Sigma^+$ state into the $3^1\Sigma^+$ state (similar studies on a three-level model system but including optimization of the frequency dispersed TAS in different chosen frequency windows can be found in [12]). By optimizing the exciting laser pulse, the TAS could be maximized, and its dependence on the probe pulse length and central frequency has been analyzed. For this, a modified iteration scheme solving the control task has been used such that the pump pulse (control pulse) energy could be fixed a priori. The probe pulse TAS increases with the probe pulse length. Because the vibrational dynamics prevents the localization of the vibrational wave packet, the increase of the signal is slower than for the case of impulsive excitations. However, there exist an optimal central frequency of the probe-pulse ($\hbar\omega_{\mathrm{pr}} \approx 0.87$ eV) such that the behavior of impulsive excitation last up to $\tau_{\mathrm{pr}} \approx 50$ fs. Setting the central frequency more off-resonant, then the absorption signal decreases even after a probe pulse length of 30 fs. And, the possibility was demonstrated to form a localized or at least a highly concentrated vibrational wave packet in the first-excited electronic NaK state. By selecting the central frequency of the probe pulse appropriately, the vibrational wave packet can be set either at the border or within the potential energy surface (PES) of the first-excited state while the probe pulse acts. For the first case the optimal pump pulse forms one vibrational wave packet which is shaped during further excitations. The second case is realized by creating two subsequent vibrational wave packets. The temporal distance is such that the first wave packet, which is reflected from the right border of the PES, interferes with the second one leading to a localized vibrational wave packet at an appropriate position for excitations into the second-excited state.

To summarize, the presented studies clearly underline the possibility to account within numerical simulations for more involved control tasks. This would be one step further towards matching the peculiarities of respective experiments.

Acknowledgments

References

[1] J.L. Herek, W. Wohlleben, R.J. Cogdell, D. Zeidler, M. Motzkus, Nature 417 (2002) 533.
[2] D. Zeidler, S. Frey, W. Wohlleben, M. Motzkus, F. Busch, T. Chen, W. Kiefer, A. Materny, J. Chem. Phys. 116 (2002) 5231.
[3] T. Brixner, N.H. Damrauer, B. Kiefer, G. Gerber, J. Chem. Phys. 118 (2003) 3692.
[4] G. Vogt, G. Krampert, P. Niklaus, P. Nuernberger, G. Gerber, Phys. Rev. Lett. 94 (2005) 068305.
[5] C. Daniel, J. Full, L. González, C. Lupulescu, J. Manz, A. Merli, S. Vajda, L. Wöste, Science 299 (2003) 536.
[6] B. Schäfer-Bung, R. Mitrić, V. Bonačić-Koutecký, A. Bartelt, C. Lupulescu, A. Lindinger, Š. Vajda, S.M. Weber, L. Wöste, J. Phys. Chem. A 108 (2004) 4175.
[7] Th. Hornung, M. Motzkus, R. de Vivie–Riedle, J. Chem. Phys. 115 (2001) 3105.
[8] I.R. Sola, H. Rabitz, J. Chem. Phys. 120 (2004) 9009.
[9] B. Brüggemann, V. May, J. Phys. Chem. B 108 (2004) 10529.
[10] T. Mancal, V. May, Chem. Phys. Lett. 362 (2002) 407.
[11] A. Kaiser, V. May, J. Chem. Phys. 121 (2004) 2528.
[12] A. Kaiser, V. May, Chem. Phys. Lett. 405 (2005) 339.
[13] A.P. Pierce, M.A. Dahleh, H. Rabitz, Phys. Rev. A 37 (1988) 4950.
[14] S.A. Rice, M. Zhao, Optical Control of Molecular Dynamics, Wiley, New York, 2000.
[15] M. Shapiro, P. Brumer, Principles of the Quantum Control of Molecular Processes, Wiley, New Jersey, 2003.
[16] V. May, O. Kühn, Charge and Energy Transfer Dynamics in Molecular Systems, Wiley–VCH, Berlin, 2004.
[17] W. Zhu, J. Botina, H. Rabitz, J. Chem. Phys. 108 (1998) 1953.
[18] W. Zhu, H. Rabitz, J. Chem. Phys. 109 (1998) 385.
[19] S.H. Tersigni, P. Gaspard, S.A. Rice, J. Chem. Phys. 114 (1990) 1670.
[20] M. Demiralp, H. Rabitz, Phys. Rev. A 47 (1993) 809, and 57 (1998) 2420.
[21] Y. Ohtsuki, K. Nakagami, Y. Fuijimura, W. Zhu, H. Rabitz, J. Chem. Phys. 114 (2001) 8867.
[22] Y. Ohtsuki, G. Turinici, H. Rabitz, J. Chem. Phys. 120 (2004) 5509.
[23] S. Shi, H. Rabitz, J. Chem. Phys. 92 (1990) 364, and 97 (1992) 276.
[24] H. Zhang, H. Rabitz, J. Chem. Phys. 101 (1994) 8580, and 97 (1992) 276.
[25] S. Magnier, M. Aubert-Frécon, Ph. Millié, J. Mol. Spectrosc. 200 (2000) 96.
[26] Of course the neglect of rotational transitions in the course of optical excitation seems rather crude. But having a ensemble of polyatomic molecules with random orientation in mind the presented studies on the applicability of OCT are rather useful.